Monthly Notices
of the
ROYAL ASTRONOMICAL SOCIETY

MNRAS **444,** 117–128 (2014) doi:10.1093/mnras/stu1402

A reassessment of the redshift distribution and physical properties of luminous (sub-)millimetre galaxies

M. P. Koprowski,[1]★ J. S. Dunlop,[1] M. J. Michałowski,[1,2]† M. Cirasuolo[1,3] and R. A. A. Bowler[1]

[1]*SUPA‡, Institute for Astronomy, University of Edinburgh, Royal Observatory, Edinburgh EH9 3HJ, UK*
[2]*Sterrenkundig Observatorium, Universiteit Gent, Krijgslaan 281 S9, B-9000 Gent, Belgium*
[3]*UK Astronomy Technology Centre, Royal Observatory, Edinburgh EH9 3HJ, UK*

Accepted 2014 July 9. Received 2014 July 9; in original form 2013 December 6

ABSTRACT

Motivated by the current controversy over the redshift distribution and physical properties of luminous (sub-)mm sources, we have undertaken a new study of the brightest sample of unlensed (sub-)mm sources with pre-Atacama Large Millimeter/submillimeter Array (ALMA) interferometric follow-up in the Cosmological Evolution Survey field. Exploiting the very latest multifrequency supporting data, we find that this sample displays a redshift distribution indistinguishable from that of the lensed sources uncovered with the South Pole Telescope, with $z_{\rm median} \simeq 3.5$. We also find that, over the redshift range $z \simeq 2$–6, the median stellar mass of the most luminous (sub-) mm sources is $M_* \simeq 3 \times 10^{11}\,{\rm M}_\odot$, yielding a typical specific star formation rate sSFR $\simeq 3\,{\rm Gyr}^{-1}$. Consistent with recent ALMA and the Submillimeter Array studies, we confirm that source blending is *not* a serious issue in the study of luminous (sub-) mm sources uncovered by ground-based, single-dish surveys; only $\simeq$10–15 per cent of bright ($S_{850} \simeq 5$–10 mJy) (sub-) mm sources arise from significant (i.e. >20 per cent) blends, and so our conclusions are largely unaffected by whether we adopt the original single-dish mm/sub-mm flux densities/positions or the interferometric data. Our results suggest that apparent disagreements over the redshift distribution of (sub-)mm sources are a result of 'down-sizing' in dust-enshrouded star formation, consistent with existing knowledge of the star formation histories of massive galaxies. They also indicate that extreme star-forming galaxies at high redshift are, on average, subject to the same star formation rate-limiting processes as less luminous objects, and lie on the 'main sequence' of star-forming galaxies at $z > 3$.

Key words: galaxies: active – galaxies: evolution – galaxies: high-redshift – galaxies: starburst – cosmology: observations – submillimetre: galaxies.

1 INTRODUCTION

Since their discovery 15 years ago in the first blank-field Submillimetre Common-User Bolometer Array (SCUBA) surveys at the James Clerk Maxwell Telescope, it has been known that sub-mm sources selected at high galactic latitudes are luminous dust-enshrouded star-forming galaxies, primarily located at high redshifts ($1 < z < 5$; Barger et al. 1998; Hughes et al. 1998). Indeed, in a hint of things to come, it was quickly realized that the brightest sub-mm source uncovered in the first 850 μm image of the *Hubble Deep Field*-North, HDF850.1, was not visible in the ultra-deep *Hubble Space Telescope* (*HST*) optical imaging then available, and a number of follow-up studies suggested that it most likely lay at $z > 4$ (Downes et al. 1999; Dunlop et al. 2004; Cowie et al. 2009). Recently, in an impressive demonstration of the ever-improving capabilities of mm/sub-mm spectroscopy, HDF850.1 has been revealed to lie at $z = 5.2$ (Walter et al. 2012).

Despite the fairly extreme redshift of the first blank-field sub-mm source ever discovered, improved and expanded sub-mm/mm surveys over the last decade undertaken with SCUBA, Large Apex Bolometer Camera (LABOCA), Astronomical Thermal Emission Camera (AzTEC) and Max Plank Millimeter Bolometer (MAMBO) have generally yielded a consistent picture, whereby sources selected at $S_{850} \simeq 5$ mJy display a redshift distribution which peaks at $z \simeq 2.5$, albeit with a significant lower redshift tail

★ E-mail: mpk@roe.ac.uk
† FWO Pegasus Marie Curie Fellow.
‡ Scottish Universities Physics Alliance

down to $z \simeq 1$ and a high-redshift tail extending up to $z \simeq 4$–5. In general, this information has been gleaned from either optical spectroscopic redshifts (e.g. Chapman et al. 2003, 2005) or from (more complete, but less accurate) optical–infrared photometric redshifts (e.g. Clements et al. 2008; Dye et al. 2008; Chapin et al. 2009; Dunlop et al. 2010; Wardlow et al. 2011; Michałowski et al. 2012a) derived for the galaxy counterparts identified via the improved spatial information provided by radio and/or *Spitzer* observations of the (sub-)mm sources (e.g. Ivison et al. 2007; Biggs et al. 2011; Michałowski et al. 2012a; Yun et al. 2012). The determination of redshifts from optical spectroscopy is well known to be difficult in the 'redshift desert' at $1.5 < z < 2.0$ (due to the lack of emission lines accessible to silicon-based detectors) and even at higher redshifts success is by no means guaranteed for sub-mm galaxies (SMGs), given the ease with which Lyman α emission can be extinguished by dust. Nevertheless, a sufficient number of spectroscopic redshifts have been measured to confirm the reliability of photometric redshift determination for sub-mm sources, and typically $\simeq$80 per cent of sub-mm sources in blank-field surveys can now be successfully associated with a galaxy counterpart (e.g. Ivison et al. 2007; Lindner et al. 2011; Michałowski et al. 2012a). Thus, despite the fact that radio and mid-infrared galaxy counterpart detection becomes increasingly difficult with increasing redshift (unlike sub-mm/mm detection), there appears to be limited room for a substantial extreme-redshift population in the typical sub-mm/mm galaxy samples studied to date. Indeed, the relatively modest disagreements between the redshift distributions of existing SMG samples can be attributed to cosmic variance (Michałowski et al. 2012a).

Now, however, a new generation of facilities is being utilized. First, *Herschel* and the South Pole Telescope (SPT) have now delivered sufficiently large far-infrared/mm maps to uncover examples of rare, very bright, generally lensed objects, for which follow-up molecular spectroscopy has proved feasible with Atacama Large Millimeter/submillimeter Array (ALMA) and the latest generation of wide-bandwidth redshift receivers on single-dish (sub-)mm telescopes. For example, pre-selection of red sources from *Herschel* data has yielded a new redshift record of $z = 6.34$ for a sub-mm-selected galaxy (Riechers et al. 2013), while ALMA follow-up of a bright sample of lensed sources uncovered with the SPT has yielded a redshift distribution which apparently peaks at $z > 3$ (Vieira et al. 2013; Weiss et al. 2013). In parallel with these sub-mm/mm spectroscopic studies of bright lensed sources, ALMA has also recently been used to undertake a systematic imaging study of unlensed sources in the *Chandra Deep Field*-South (Hodge et al. 2013; Karim et al. 2013), as originally uncovered in the LABOCA LESS survey (Weiss et al. 2009).

These new studies have produced results which some have regarded as casting doubt on our existing knowledge of the (sub-)mm source population. First, it has been claimed that the (apparently robustly established) redshift distribution of (sub-)mm sources has been biased low (Vieira et al. 2013), questioning the reliability of the aforementioned galaxy identification techniques based on the supporting radio-near/mid-infrared imaging. Secondly, it has been suggested that a substantial fraction of bright (sub-)mm sources in single-dish surveys arise from blends, raising additional concerns about the effectiveness of identification methods applied to large-beam sub-mm maps (Wang et al. 2011; Hodge et al. 2013; Karim et al. 2013).

The first of these claims might seem surprising, given the high completeness of galaxy identifications in previous blank-field surveys and the robustness of photometric redshifts (consistently yielding $z_{\rm median} \simeq 2.5$). Nevertheless, by the end of 2012, over 10 SMGs had already been spectroscopically confirmed at $z > 4$ (Capak et al. 2008, 2011; Schinnerer et al. 2008; Coppin et al. 2009; Daddi et al. 2009a,b; Knudsen et al. 2009; Riechers et al. 2010; Cox et al. 2011; Smolcic et al. 2011; Combes et al. 2012; Walter et al. 2012), and it has been suggested by several authors that the most luminous sub-mm/mm galaxies appeared to lie at preferentially higher redshifts than their more moderate-luminosity counterparts (e.g. Wall, Pope & Scott 2008; Dunlop 2011; Ivison et al. 2002; Michałowski et al. 2012a). The second claim, regarding prevalent source blending, seems equally surprising given that previous sub-mm/mm interferometry with the Submillimeter Array (SMA) and Plateau de Bure Interferometer (PdBI) interferometers had suggested that serious multiplicity was not a big issue (e.g. Iono et al. 2006; Younger et al. 2007, 2008, 2009; Hatsukade et al. 2010).

Motivated by this controversy and confusion, and by the ever-improving multifrequency data set in the Cosmological Evolution Survey (COSMOS) field (including UltraVISTA; Bowler et al. 2012; McCracken et al. 2012), we have undertaken a fresh investigation of the properties of bright (but unlensed) sub-mm/mm galaxies as selected from the largest flux-limited sub-mm sample with pre-ALMA interferometric follow-up observations. Our sample consists of the 30 brightest sub-mm/mm sources in the COSMOS field which were originally uncovered with AzTEC and LABOCA, and which have subsequently been imaged with the SMA (Younger et al. 2007, 2009) and the PdBI (Smolcic et al. 2012). Our aim was to combine the $\simeq$0.2 positional accuracy delivered by the sub-mm/mm interferometry, with the latest Subaru, UltraVISTA and *Spitzer* optical–infrared photometry to unambiguously establish the galaxy identifications, redshifts (z), stellar masses (M_*) and specific star formation rates (sSFR) for a well-defined sample of bright sub-mm sources. At the same time, we have taken the opportunity to revisit the issue of source multiplicity, and the robustness of galaxy identifications established using the statistical associations with radio/infrared sources which would have been deduced based on the original single-dish sub-mm/mm positions.

The remainder of this paper is structured as follows. In Section 2, we describe the published (sub-)mm samples in the COSMOS field with interferometric follow-up, and summarize the latest multifrequency data that we have used to uncover and study the galaxies which produce the detected sub-mm/mm emission. Next, in Section 3, we describe the process of galaxy identification, and the extraction of robust optical–infrared multiwavelength photometry. Then, in Section 4 we present and discuss the derived properties of the galaxies, with special emphasis on the derived redshift distribution of bright (sub-)mm sources and the stellar masses of the associated galaxies. In Section 5, we consider further our findings in the context of the latest *Herschel*/SPT/ALMA studies detailed above, and include a reassessment of how reliably galaxy counterparts can actually be established purely on the basis of the original single-dish sub-mm/mm maps (and hence to what extent higher resolution sub-mm/mm imaging impacts on our understanding of the SMG population). Our conclusions are summarized in Section 6.

Throughout we use the AB magnitude system (Oke 1974), and assume a flat cosmology with $\Omega_{\rm m} = 0.3$, $\Omega_\Lambda = 0.7$ and $H_0 = 70$ km s^{-1} Mpc^{-1}.

2 DATA

The AzTEC/COSMOS survey covers 0.15 deg^2 of the COSMOS field at 1.1 mm with an rms noise of 1.3 mJy beam^{-1} (Scott et al. 2008). The published AzTEC/COSMOS catalogue consists

of 44 sources with S/N $\geq 3.5\sigma$. The brightest 15 of these sources were then followed up with the SMA (Younger et al. 2007, 2009), effectively yielding a flux-limited sample of millimetre-selected galaxies with refined positions. All 15 of these sources were detected with the SMA, providing submillimetre positions accurate to $\simeq$0.2 arcsec (see Table 3). Two of the sources were split by the SMA into two distinct components; AzTEC11 was subdivided into north and south components and AzTEC14 into west and east. In the case of AzTEC11 however, as can be seen from fig. 1 of Younger et al. (2009), the resolution of the SMA image is not high enough to clearly separate the components. For this reason, we decided to continue to treat AzTEC11 as a single (albeit somewhat extended) galaxy for the purpose of this study.

The LABOCA/COSMOS survey covers the inner $\simeq$0.7 deg^2 of the COSMOS field, delivering a submillimetre map at $\lambda = 870$ μm with an rms noise level of 1.5 mJy beam^{-1} (Navarrete et al., in preparation). The 28 brightest 870 μm sources were chosen for Institut de Radioastronomie Millimetrique (IRAM) PdBI follow-up observations with the requirement that the signal-to-noise S/N$_{\rm LABOCA} \gtrsim 3.8$ (Smolcic et al. 2012). Most of these were detected with the IRAM interferometer. To create a well-defined and (near) flux-limited sample for the present study, we selected the 16 objects with S/N$_{\rm PdBI}$ $\gtrsim$ 4.0. These are listed in Table 4. However, as described in the notes on individual sources in Appendix A, the PdBI position of COSLA-38 is so far from the original LABOCA position, and so close to the edge of the beam that it is hard to be confident it is the same source. For this reason, we have excluded COSLA-38, and all further analysis is thus performed on a final sample of 30 (sub-)mm sources.

We used the refined positions provided by the SMA and PdBI interferometry to identify galaxy counterparts in the available multifrequency imaging. The location of the AzTEC/SMA and LABOCA/PdBI sources within the key available multiwavelength imaging in the COSMOS field is illustrated in Fig. 1.

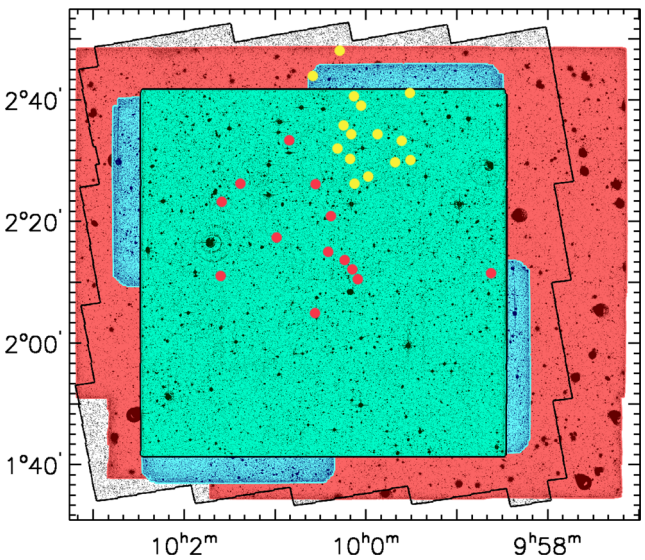

Figure 1. The location of the 30 (sub-)mm sources studied here within the multiband coverage of the COSMOS field. The x and y axes are RA and Dec., respectively. From the outside, the red area is the 1.5 deg^2 UltraVISTA field, the irregular black outline delineates the *HST*/ACS f_{814}-band imaging, the blue region is the Subaru z'-band Suprime-Cam mosaic and the innermost green area marks the CFHTLS D2 optical data. Yellow and red dots indicate the positions of the AzTEC and LABOCA sources, respectively (figure adapted from Bowler et al. 2012).

Table 1. A summary of the optical and near-infrared imaging data utilized in this study. Column 1 gives the filter bandpass names, column 2 their effective wavelengths, column 3 the FWHM of the bandpasses, column 4 gives the 5σ photometric depths (AB mag) within a 2 arcsec diameter aperture and column 5 gives the seeing in arcsec. The u, g, r, i imaging was delivered by the CFHT Legacy Survey, the z' imaging was obtained with the refurbished Suprime-Cam on Subaru (Bowler et al. 2012; Furusawa et al., in preparation) while the Y, J, H, K_s imaging was provided by UltraVISTA DR1 (McCracken et al. 2012).

Filter	$\lambda_{\rm eff}$/nm	FWHM/nm	5σ/AB mag	seeing/arcsec
u	381.1	65.2	26.9	0.80
g	486.2	143.6	27.0	0.65
r	625.8	121.7	26.6	0.65
i	769.0	137.0	26.4	0.65
z'	903.7	85.6	26.3	1.15
Y	1020	100	24.7	0.82
J	1250	180	24.5	0.79
H	1650	300	24.0	0.76
K_s	2150	300	23.8	0.75

Table 2. A summary of the wider area Subaru optical imaging (Taniguchi et al. 2007) utilized in the study of AzTEC7 and AzTEC12. Column 1 gives the filter bandpass names, column 2 their effective wavelengths, column 3 the FWHM of the bandpasses, column 4 gives the 5σ photometric depths (AB mag) within a 2 arcsec diameter aperture and column 5 gives the seeing in arcsec.

Filter	$\lambda_{\rm eff}$/nm	FWHM/nm	5σ/AB mag	seeing/arcsec
B	446.0	89.7	27.14	0.95
V	548.4	94.6	26.75	1.33
g'	478.0	126.5	27.26	1.58
i'	764.1	149.7	26.08	0.95
r'	629.5	138.2	26.76	1.05
z'	903.7	85.6	26.00	1.15

This imaging consists of the public Infrared Array Camera (IRAC) imaging obtained via the S-COSMOS survey (Sanders et al. 2007), the new near-infrared imaging provided by UltraVISTA DR1 (McCracken et al. 2012), and optical imaging from the Canada–France–Hawaii Telescope (CFHT) Legacy Survey (CFHTLS; Gwyn 2011) and Subaru (Taniguchi et al. 2007; Furusawa et al., in preparation). The details of this imaging are summarized in Tables 1 and 2, with the latter table being relevant for AzTEC7 and AzTEC12 which lie just outside the deep CFHT MegaCam pointing (see Fig. 1), and thus required use of the (somewhat shallower) Subaru imaging available over the whole COSMOS field.

3 GALAXY COUNTERPARTS AND MULTIWAVELENGTH PHOTOMETRY

Initially we searched for galaxy counterparts in the UltraVISTA DR1 K_s-band imaging, using a (deliberately generous) search radius of 3 arcsec around the interferometric (sub-)mm positions. Near-infrared counterparts were found for all of the (sub-)mm sources except for AzTEC14.W, COSLA-6N, COSLA-17S and COSLA-128. However, as can be seen in Fig. 2, for AzTEC2 (A2.S), 13, 14.E, COSLA-8, 19 and 23S, the (sub-)mm-to-K_s positional offset is too large for the association to be trusted. Also, for the reasons detailed in the 'Notes on individual objects' (available in the

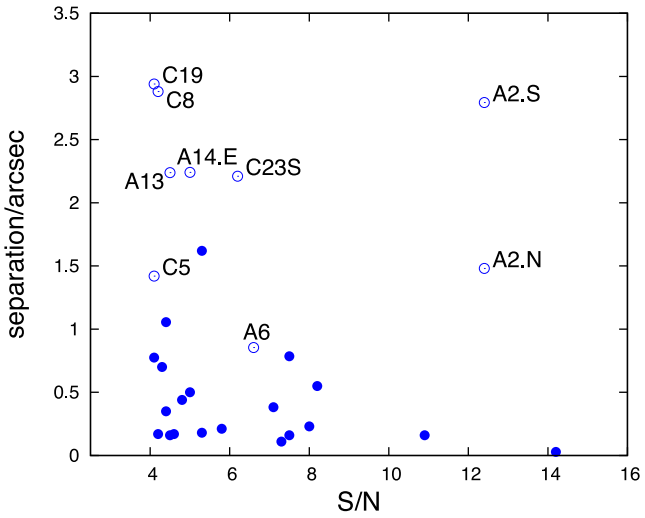

Figure 2. The interferometric S/N of each (sub-)mm detection is plotted here as a function of angular separation between the (sub-)mm interferometric position and the nearest potential near-infrared/optical counterpart in the available imaging. The empty circles represent objects for which we regard the multifrequency match as incorrect given the positional accuracy delivered by the interferometry (i.e. all objects with a separation >2 arcsec). AzTEC2 was initially matched to a bright foreground galaxy (A2.S) in the wings of which a fainter, possibly lensed object was discovered (A2.N) after careful image analysis. However, because the radio counterpart of AzTEC2 is exactly at the position of the SMA ID, both these possible near-infrared counterparts can be excluded. COSLA-5 was matched to an optical object (C5), as was AzTEC6 (A6), for which Smolcic et al. (2012) derived photometric redshifts of $z_{\rm est} \simeq 0.85$ and $z_{\rm est} \simeq 0.82$, respectively. However, these relatively low-redshift possible identifications can be excluded due to the lack of any radio detections in the available VLA 1.4 GHz imaging, which securely places the (sub-)mm sources at higher redshifts (at least $z > 1.5$; see Fig. 4, and Notes on individual objects in Appendix A). All the unlabelled objects are summarized in Tables B2 and B3 available in the online version. The blue filled dot with a separation of 1.62 arcsec is our optical counterpart for AzTEC10, which we selected on the basis of 8 μm flux density and $i - K$ colour. The filled blue dot with a separation of 1.05 arcsec indicates our chosen identification for AzTEC15.

online version), the optical/infrared counterparts labelled A2.N, A6 and C5 were also not deemed reliable. This leaves a total of 18/30 (sub-)mm sources with robust near-infrared galaxy counterparts (note that in Section 5.2 we discuss the extent to which the same galaxy counterparts would have been identified without the availability of (sub-)mm interferometric observations).

After ensuring that all the optical–infrared imaging was accurately astrometrically aligned to the K_s-band imaging (see Bowler et al. 2012), multiband aperture photometry was performed at all available wavelengths through 2 arcsec diameter apertures, with multiple 2 arcsec diameter apertures placed on blank-sky regions within ≃30 arcsec of the source in order to reliably estimate the local photometric uncertainty in each band. With the obvious exception of the IRAC imaging, the imaging data are fairly well matched in terms of seeing quality, but all aperture magnitudes were subsequently corrected to total utilizing the measured point spread function in each band. Photometry in the IRAC bands was taken from the S-COSMOS imaging, again corrected to total assuming that the sources were not significantly resolved at IRAC wavelengths. The final multiband photometry measured for the 18 sources with reliable optical–infrared galaxy counterparts is detailed in Tables B2 and B3 (available in the online version).

4 SOURCE PROPERTIES

4.1 Photometric redshifts

The multiband photometry described above was used to derive photometric redshifts using a χ^2 minimization method (Cirasuolo et al. 2007, 2010) with a code based on the HYPERZ package (Bolzonella, Miralles & Pelló 2000). To create templates of galaxies, the stellar population synthesis models of Bruzual & Charlot (2003) were applied, using the Chabrier (2003) stellar initial mass function (IMF) with a lower and upper mass cut-off of 0.1 and 100 $M_\odot$, respectively. A double-burst star formation history with a fixed solar metallicity was used. Dust reddening was taken into account using the Calzetti et al. (2000) law within the range $0 \leq A_V \leq 6$. The H I absorption along the line of sight was applied according to Madau (1995).

For the (sub-)mm sources for which no optical near-infrared counterpart was found in the available imaging, long-wavelength photometric redshift estimates were derived from their 24 μm to 20 cm spectral energy distributions (SEDs; including the radio flux densities given by Smolcic et al. 2012) using the average SMG spectral template derived by Michałowski, Hjorth & Watson (2010). Given the potential complications of dust temperature varying with redshift (e.g. Aretxaga et al. 2007; Amblard et al. 2010; Hwang et al. 2010), we experimented with various template libraries, but found that the strongest correlation between redshifts derived from the long-wavelength data and the known optical–near-infrared redshifts (either spectroscopic or photometrically estimated) was achieved by fitting the long-wavelength data with this average template (see Fig. 3). Thus, treating the shorter wavelength redshift information as a training set, we adopted values for $z_{\rm LW}$ based on fitting the far-infrared–radio data with the Michałowski et al. (2010) template, and these are the values listed in column 4 of Table 5.

The resulting redshift measurements and estimates are summarized in Table 5. As a basic test of the reliability of our redshift estimates, we compare (in Fig. 3) our photometric redshifts with the spectroscopic measurements for the five sources in our sample for which reliable optical spectroscopy of the current galaxy counterparts has been obtained (Smolcic et al. 2012); the mean offset is $\Delta z/(1 + z_{\rm spec}) = 0.009 \pm 0.026$, consistent with zero. In the lower panel of this figure, we compare our optical/near-infrared photometric redshift estimates with our long-wavelength photometric redshifts for those sources for which both estimates are available. This shows that the $z_{\rm LW}$ redshift estimates are certainly consistent with the optical/near-infrared photometric redshifts, albeit with more scatter and with a trend for some high-redshift sources to have redshift underestimated by $z_{\rm LW}$. This suggests that at least some of the most distant (sub-)mm galaxies in our sample may have higher dust temperatures compared to the average $z \simeq$ 2–3 (sub-)mm galaxies SED template utilized here to derive $z_{\rm LW}$.

In Fig. 4, we plot our objects on the redshift–millimetre/radio flux-density ratio plane, both using our own final redshifts (from Table 5) and using the redshifts given for these same objects by Smolcic et al. (2012, given in column 4 of Table 5). We plot the redshift information in this way both to clarify the extent to which our redshift estimates differ from those adopted by Smolcic et al. (2012) on a source-by-source basis and to demonstrate that all our adopted redshifts ($z_{\rm spec}$, or failing that $z_{\rm phot}$ or failing that $z_{\rm LW}$) are consistent with the anticipated redshift dependence of the millimetre/radio flux-density ratio displayed by a reasonable range of template long-wavelength SEDs (as detailed in the plot legend). This plot serves to emphasize that the redshifts given for at least

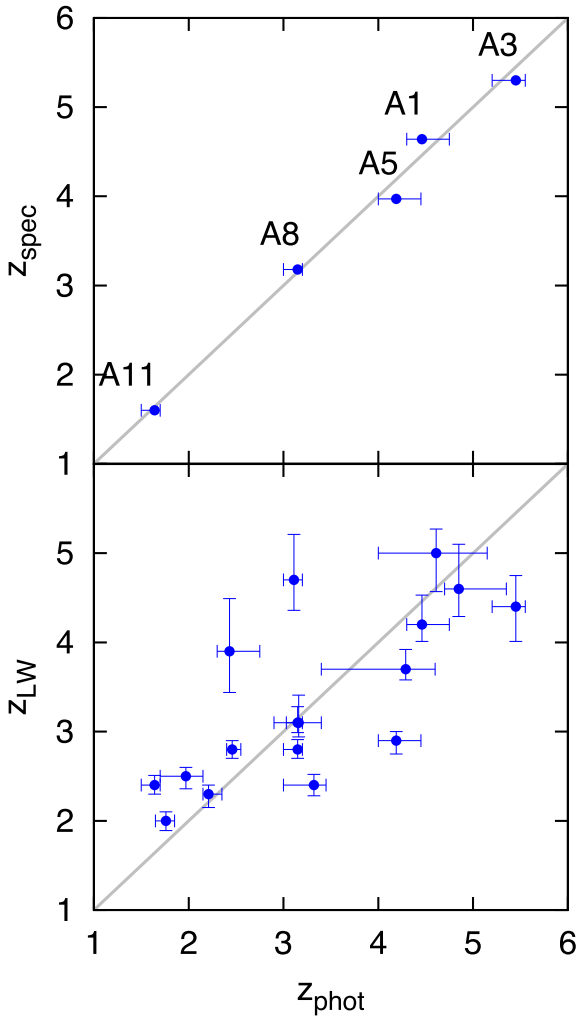

Figure 3. Upper panel: our optical/near-infrared photometric redshifts plotted versus the spectroscopic redshifts for the five sources with reliable spectroscopy (Smolcic et al. 2012), demonstrating the accuracy of z_{phot}. Lower panel: the optical/near-infrared photometric redshifts (z_{phot}) are compared with our long-wavelength mm/radio estimates (z_{LW}) for those objects for which both measurements are possible (see Table 5) in order to check for accuracy and potential bias; the significantly greater uncertainty in z_{LW} is apparent, but the mean value of z_{phot}/z_{LW} is 1.2 ± 0.36, consistent with unity, and thus indicating no major systematic bias.

six (and more likely eight) of these (sub-)mm sources by Smolcic et al. (2012) are clearly incorrect, as the resulting flux-density ratios are inconsistent with (i.e. much larger than) even extreme choices of cool SEDs at the relevant redshifts. The interested reader can find the details for these differences in the Notes on individual objects available in the online version, which can be usefully read in conjunction with Fig. 4.

4.2 Redshift distribution

The differential redshift distribution derived for our complete 30-source sample is presented in Fig. 5, where it is compared with several recently published redshift distributions for (sub-)mm source samples. The median redshift derived for our COSMOS sample is $z_{med} = 3.44 \pm 0.16$, whereas for the AzTEC/SHADES sample it is $z_{med} = 1.89 \pm 0.06$ (Michałowski et al. 2012a), and for the sample of Chapman et al. (2005), $z_{med} = 2.14 \pm 0.06$. Clearly, the redshift distribution of our (sub-)mm sample lies at somewhat higher redshift than the majority of recently published redshift distributions for (sub-)mm-selected samples. In part this could be due to the fact that there are no obvious biases in the identification techniques used here, whereas several previously published redshift distributions contain only sources with robust radio identifications. However, as we explore further below, it may also be due to the fact that the sample considered here is confined to significantly more luminous (sub-)mm sources than, for example, the source samples considered by Michałowski et al. (2012a), or Yun et al. (2012), or Simpson et al. (2014). We re-emphasize that, despite the fact that most of the (sub-)mm sources are in common, our redshift distribution lies at significantly higher redshift than that published by Smolcic et al. (2012); as discussed above (and detailed in Fig. 4) in part this is undoubtedly due to our rejection of several of the lower redshift candidate identifications proposed by Smolcic et al. (2012), but it is also in part a result of our deliberate exclusion of some of the less luminous LABOCA/PdBI sources in an effort to achieve a homogeneous bright source sample.

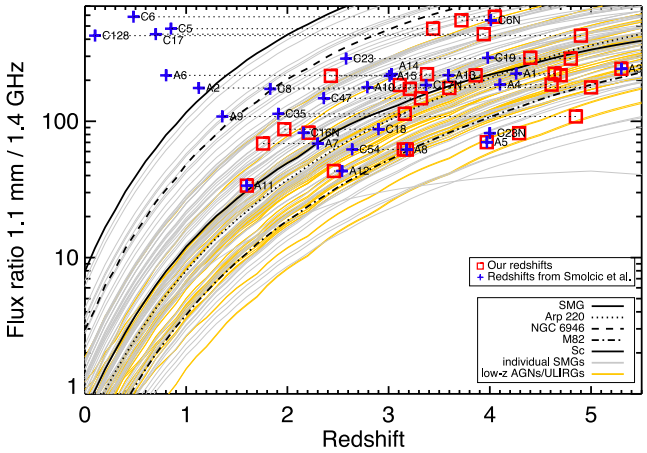

Figure 4. The millimetre/radio flux-density ratio of the 30 COSMOS (sub-)mm sources plotted against their redshifts as derived in the present study (red squares) and in the previous study by Smolcic et al. (2012, blue crosses). These data points showing the positions of the individual sources on this diagram are overlaid on a range of curves indicating the expected redshift dependence of the observed value of the 1.1 mm/1.4 GHz flux-density ratio as derived from a wide range of observed galaxy SEDs (figure adapted from Michałowski et al. 2012a). This plot serves to illustrate three key points. First, it shows that the redshifts derived here (whether spectroscopic redshifts, optical–near-infrared photometric estimates or long-wavelength SED fits) all result in reasonable values for the mm/radio flux-density ratios. Secondly, it is clear that the redshifts adopted by Smolcic et al. (2012) for at least six of the sources are implausible, in the sense that they are inconsistent with the form of any plausible long-wavelength SED. Thirdly, by connecting the alternative redshift estimates of each source with dotted lines, it is made clear which sources have had their redshifts most dramatically revised in the current work (see also the Notes on individual sources in the online version).

Interestingly, as shown in Fig. 6, the redshift distribution derived here is basically identical to that produced by Vieira et al. (2013) from their ALMA follow-up CO spectroscopy of the lensed mm-selected galaxy sample from the SPT [the Kolmogorov-Smirnov (K-S) test yields $p = 0.991$]. This is potentially important because, until now, it has been claimed that the SPT redshift distribution is inconsistent with any (sub-)mm source redshift distribution derived without the benefit of ALMA CO spectroscopy (see Vieira et al. 2013).

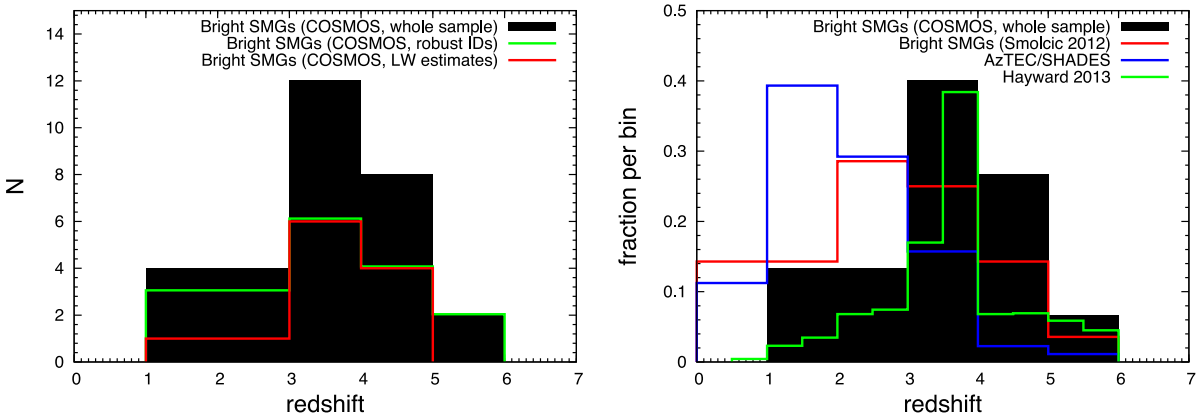

Figure 5. Left-hand panel: the redshift distribution of our full 30-source sample of luminous (sub-)mm sources in the COSMOS field (Table 5). The mean redshift is $\bar{z} = 3.53 \pm 0.19$. Where available, optical spectroscopic redshifts ($z_{\rm spec}$) have been used (5 sources), with optical/near-infrared photometric estimates ($z_{\rm phot}$) then used where judged robust (13 sources), and long-wavelength redshift estimates ($z_{\rm LW}$) adopted for the remaining objects (12 sources). Right-hand panel: redshift distribution for the whole COSMOS sample with overlaid distributions derived for the COSMOS sources by Smolcic et al. (2012, $\bar{z} = 2.8 \pm 0.3$) and for the robust galaxy identifications in the AzTEC/SHADES survey presented by Michałowski et al. (2012a, $\bar{z} = 2.0 \pm 0.1$). In addition, we plot the Hayward et al. (2013) simulated redshift distribution for mm-selected sources with $F_{1.1\ {\rm mm}} > 4$ mJy, which is consistent with the observed redshift distribution presented here for comparably luminous sources.

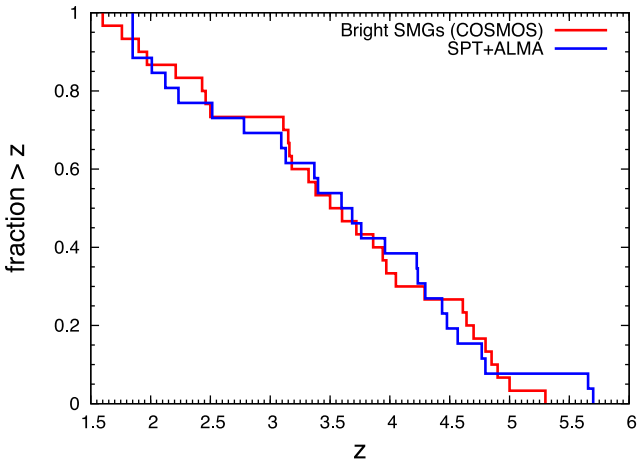

Figure 6. A comparison of our estimated cumulative redshift distribution for the bright 30-source COSMOS sample considered here and that published by Vieira et al. (2013) from ALMA follow-up CO spectroscopy of the lensed mm sources uncovered by the SPT. It is visually obvious that the redshift distributions are indistinguishable, and indeed application of the K-S test yields a significance value $p = 0.991$.

It is reassuring that these two redshift distributions are so clearly consistent, as it is hard to imagine that our rather robust and well-validated photometric redshift estimation techniques should yield a significantly biased redshift distribution. However, it needs to be explained why the sample studied here yields a redshift distribution consistent with the SPT results, while most other studies of (sub-)mm galaxies clearly do not. As justified further below, we believe there is good evidence that this is primarily a result of 'downsizing' in the star-forming population, and that both our COSMOS sample and the SPT sample are biased to significantly higher luminosity sources than most other studies (e.g. Michałowski et al. 2012a; Simpson et al. 2014; Swinbank et al. 2014). Of course, part of the reason the SPT sources are so *apparently* bright is that they are lensed, but it transpires that in general the lensing factors are not sufficiently extreme to remove the overall bias of the bright/large SPT survey towards the most intrinsically luminous mm sources [for example, the de-lensed 860 μm flux densities of four SPT sources with completed lens modelling reported by Hezaveh et al. (2013) are 5, 6, 16 and 23 mJy].

The above comparison and discussion suggests that there is a correlation between (sub-)mm luminosity and mean redshift, in the sense that more luminous sources lie, on average, at systematically higher redshifts. Such a correlation has been suggested before (e.g. Dunlop et al. 1994; Ivison et al. 1998; Dunlop 2011; Michałowski et al. 2012a; Smolcic et al. 2012) and, as discussed above, provides arguably the most natural explanation for the consistency of the redshift distribution presented here with that derived from the bright SPT surveys.

In an attempt to better establish the statistical evidence for this, we plot in Fig. 7 the 1.1 mm flux density for the sources studied here and in the SHADES AzTEC survey (Michałowski et al. 2012a) versus their redshifts. A correlation is apparent, and calculation of the Spearman rank coefficient for the flux–redshift correlation yields 0.4557, rejecting the null hypothesis of no correlation with a significance value $p < 10^{-6}$. However, this result is potentially biased by the fact that it includes only the identified sources in the AzTEC/SHADES sample. When the AzTEC/SHADES sources with no secure identifications/redshifts are included (with redshifts scattered randomly between the lower limit implied by the mm/radio flux ratio and $z = 6$), the Spearman rank coefficient drops to 0.116, yielding $p = 0.025$. We thus conclude that the data do indeed support the existence of a correlation between (sub-)mm luminosity and typical redshift, but that more dynamic range and improved redshift completeness for the fainter samples are required to establish the significance and form of this relation beyond doubt.

4.3 Stellar masses and sSFR

For the 18 galaxies for which we secured a robust optical–infrared identification, we were able to use the results of the two-component SED fitting which was used to obtain photometric redshifts (see Section 4.2) to obtain an estimate of the stellar mass of each (sub-)mm-selected galaxy. As described in Michałowski et al. (2012b), we assumed a Chabrier (2003) stellar IMF, and the stellar masses are based on the models of Bruzual & Charlot (2003)

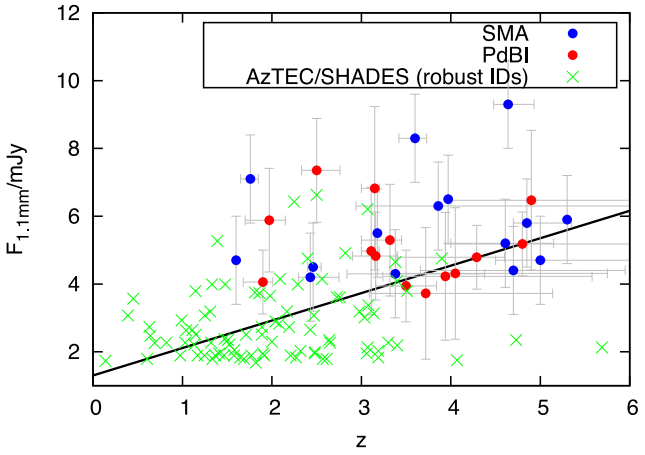

Figure 7. 1.1 mm flux density versus redshift. Red and blue dots represent our LABOCA and AzTEC samples, respectively. Black crosses are AzTEC/SHADES sources with robust galaxy counterparts (Michałowski et al. 2012b). The fluxes are those measured by the single-dish facilities, with LABOCA 870 μm flux densities converted to 1.1 mm estimated measurements assuming the mean SMG SED template of Michałowski et al. (2010). The blue line is the best-fitting straight line; $F_{1.1\ \mathrm{mm}} = (0.73 \pm 0.12)\ z + (1.73 \pm 0.33)$. The Spearman correlation coefficient is 0.4557; the resulting significance level (p) is less than 10^{-6}, indicating a highly significant correlation between redshift and mm flux density (and hence luminosity).

adopting a two-component star formation history. Where a robust spectroscopic redshift was available we adopted it, but otherwise derived the mass based on the photometric redshift. The results are tabulated in the final column of Table 5. The median stellar mass is $M_* \simeq 2.2 \times 10^{11}\,\mathrm{M}_\odot$, in excellent agreement with the average stellar mass of $z \simeq 2$ SMGs by Michałowski et al. (2012b).

We also used the redshifts and (sub-)mm flux densities of the identified sources to estimate their star formation rates (SFR). The SFRs were calculated from the (sub-)mm flux densities assuming the average (sub-)mm SED template of Michałowski et al. (2010). Due to the negative K-correction, a flux density of 1 mJy at $\lambda \simeq 1$ mm corresponds approximately to a total (bolometric) infrared luminosity of $\simeq 10^{12}\,\mathrm{L}_\odot$ at $z > 1$, which converts to SFR $\simeq 100\,\mathrm{M}_\odot\,\mathrm{yr}^{-1}$ after converting to a Chabrier (2003) IMF (Kennicutt 1998).

Armed with stellar masses and estimates of SFR, we have then proceeded to derive the specific star formation rate of each source (sSFR). The results are plotted in Fig. 8, where we show both the values derived from the original single-dish measurements and those derived assuming the interferometric flux densities. While individual values vary (see figure caption for details), it can be seen that in both cases the median value is sSFR $\simeq 2.5\,\mathrm{Gyr}^{-1}$. This is essentially identical to the average sSFR displayed by 'normal' star-forming galaxies on the 'main sequence' of star formation at $z > 2$ (e.g. Gonzalez et al. 2010; but see also Stark et al. 2013) and is again consistent with the findings of Michałowski et al. (2012b); while some subset of (sub-)mm-selected galaxies might display sSFR values which place them above the main sequence, in general they display SFRs which are perfectly consistent with the main-sequence expectation based on their high stellar masses (see also Roseboom et al. 2013).

5 SINGLE-DISH VERSUS INTERFEROMETRIC MEASUREMENTS

5.1 Multiplicity and number counts

Recently, ALMA observations of 122 870-μm sources in the Extended *Chandra Deep Field*-South from the LABOCA LESS survey (Weiss et al. 2009) have been presented, first by Karim et al. (2013), and then in more detail by Hodge et al. (2013). This sample includes 12 bright objects with original single-dish flux-density measurements of $S_{870} > 9$ mJy. From this 'ALMA LABOCA ECDFC Submm Survey (ALESS)' study, Karim et al. (2013) reported that source multiplicity is common, and that most bright (sub-)mm sources uncovered in single-dish surveys to date are in fact artificial, resulting from blends of fainter (albeit sometimes physically associated) sources within the original single-dish beam. Indeed, Karim et al. (2013) went so far as to claim that

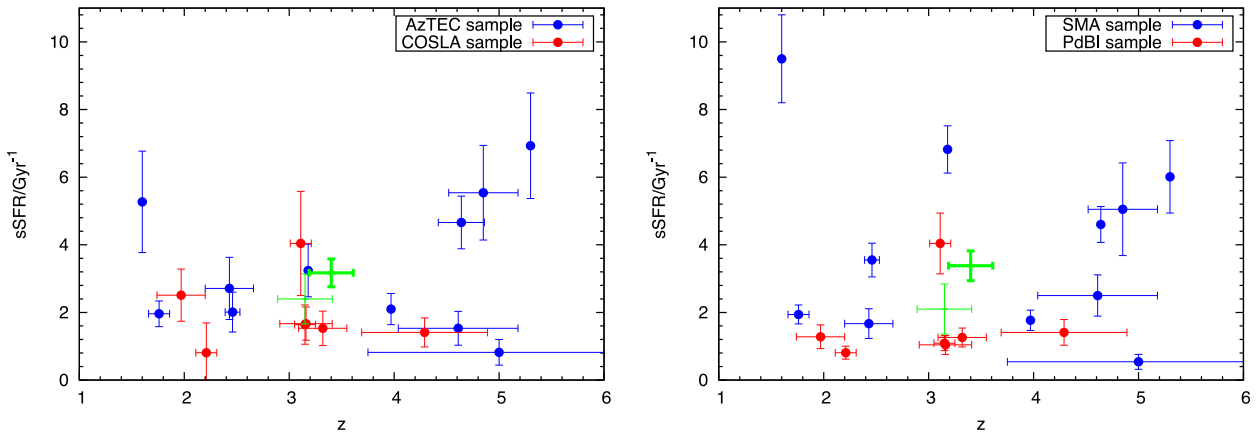

Figure 8. sSFR versus redshift. The left-hand panel shows sSFR values based on AzTEC (blue dots) and LABOCA (red dots) flux densities, while in the right-hand panel we plot sSFR values based on SMA (blue dots) and PdBI (red dots) interferometric flux densities. The green points with error bars show the median (thinner error bars) and mean (thicker error bars) values of sSFR and z in each panel; in the left-hand panel the median sSFR $= 2.40 \pm 0.74\ \mathrm{Gyr}^{-1}$ (mean sSFR $= 3.17 \pm 0.41\ \mathrm{Gyr}^{-1}$) while in the right-hand panel median sSFR $= 2.1 \pm 0.74\ \mathrm{Gyr}^{-1}$ (mean sSFR $= 3.38 \pm 0.44\ \mathrm{Gyr}^{-1}$). We conclude that the typical value of sSFR $\simeq 2.5\ \mathrm{Gyr}^{-1}$, consistent with the 'main sequence' of star-forming galaxies at $z > 2$, and that this conclusion is basically unaffected by whether we adopt the single-dish or interferometric measurements of (sub-)mm flux density. Errors on sSFR are dominated by the combined effects of the uncertainties in stellar mass (see Table 5) and the uncertainties in the long-wavelength flux-density measurements. Errors in redshifts are as given in Table 5, with no horizontal error bar visible for those sources with spectroscopic redshift measurements.

Table 3. The 15 brightest COSMOS AzTEC mm sources chosen for SMA interferometric follow-up observations which were utilized in the present study. Column 1 gives the source name, column 2 the SMA position, column 3 the SMA 890 μm signal-to-noise ratio, column 4 the AzTEC 1.1 mm signal-to-noise ratio (Younger et al. 2007, 2009), column 5 the SMA flux density and column 6 the deboosted AzTEC 1.1 mm flux density (Scott et al. 2008). AzTEC14 was resolved by the SMA into the east and west components. AzTEC11, even though it was also just resolved by the SMA into two components, is treated here as a single, extended SMG with an 890 μm flux density which is the sum of the flux densities of both components (table 1 of Younger et al. 2007).

SMA ID	SMA coords (J2000)		S/N	S/N	$F_{890\,\mu m}$	$F_{1.1\,mm}$
	RA	Dec.	SMA	AzTEC	(mJy)	(mJy)
AzTEC1	09 : 59 : 42.86	+ 02 : 29 : 38.2	14.2	8.3	15.6 ± 1.1	$9.3^{+1.3}_{-1.3}$
AzTEC2	10 : 00 : 08.05	+ 02 : 26 : 12.2	12.4	7.4	12.4 ± 1.0	$8.3^{+1.3}_{-1.3}$
AzTEC3	10 : 00 : 20.70	+ 02 : 35 : 20.5	5.8	5.9	8.7 ± 1.5	$5.9^{+1.3}_{-1.3}$
AzTEC4	09 : 59 : 31.72	+ 02 : 30 : 44.0	7.5	5.3	14.4 ± 1.9	$5.2^{+1.3}_{-1.4}$
AzTEC5	10 : 00 : 19.75	+ 02 : 32 : 04.4	7.1	6.2	9.3 ± 1.3	$6.5^{+1.2}_{-1.4}$
AzTEC6	10 : 00 : 06.50	+ 02 : 38 : 37.7	6.6	6.3	8.6 ± 1.3	$6.3^{+1.3}_{-1.2}$
AzTEC7	10 : 00 : 18.06	+ 02 : 48 : 30.5	8.0	6.4	12.0 ± 1.5	$7.1^{+1.4}_{-1.4}$
AzTEC8	09 : 59 : 59.34	+ 02 : 34 : 41.0	10.9	5.7	19.7 ± 1.8	$5.5^{+1.3}_{-1.3}$
AzTEC9	09 : 59 : 57.25	+ 02 : 27 : 30.6	4.1	5.6	9.0 ± 2.2	$5.8^{+1.3}_{-1.5}$
AzTEC10	09 : 59 : 30.76	+ 02 : 40 : 33.9	5.3	5.1	5.3 ± 1.0	$4.7^{+1.3}_{-1.3}$
AzTEC11	10 : 00 : 08.91	+ 02 : 40 : 10.2	8.2	5.1	14.4 ± 1.9	$4.7^{+1.3}_{-1.3}$
AzTEC12	10 : 00 : 35.29	+ 02 : 43 : 53.4	7.5	4.8	13.5 ± 1.8	$4.5^{+1.3}_{-1.5}$
AzTEC13	09 : 59 : 37.05	+ 02 : 33 : 20.0	4.5	4.8	8.2 ± 1.8	$4.4^{+1.3}_{-1.4}$
AzTEC14	–	–	–	4.7	–	$4.3^{-1.4}_{-1.4}$
AzTEC14.E	10 : 00 : 10.03	+ 02 : 30 : 14.7	5.0	–	5.0 ± 1.0	–
AzTEC14.W	10 : 00 : 09.63	+ 02 : 30 : 18.0	3.9	–	3.9 ± 1.0	–
AzTEC15	10 : 00 : 12.89	+ 02 : 34 : 35.7	4.4	4.6	4.4 ± 1.0	$4.2^{+1.3}_{-1.4}$

Table 4. The 16 brightest COSMOS LABOCA sub-mm sources which were followed up with the IRAM PdBI and are utilized here. Column 1 gives the source name, column 2 the PdBI position, columns 3 and 4 give the PdBI and LABOCA signal-to-noise ratios, while columns 5 and 6 give the PdBI and LABOCA flux densities. (Smolcic et al. 2012). Note that COSLA-38 was excluded from the analysis presented here due to the very large offset between the PdBI and LABOCA positions – see Notes on individual objects in Appendix A.

PdBI ID	PdBI coords (J2000)		S/N	S/N	$F_{1.3\,mm}$	$F_{870\,\mu m}$
	RA	Dec.	PdBI	LABOCA	(mJy)	(mJy)
COSLA-5	10 : 00 : 59.521	+ 02 : 17 : 02.57	4.1	5.0	2.04 ± 0.49	12.5 ± 2.6
COSLA-6N	10 : 01 : 23.640	+ 02 : 26 : 08.42	5.4	4.7	2.66 ± 0.49	16.0 ± 3.3
COSLA-6S	10 : 01 : 23.570	+ 02 : 26 : 03.62	4.8	4.7	3.08 ± 0.65	16.0 ± 3.3
COSLA-8	10 : 00 : 25.550	+ 02 : 15 : 08.44	4.2	4.6	2.65 ± 0.62	6.9 ± 1.6
COSLA-16N	10 : 00 : 51.585	+ 02 : 33 : 33.56	4.3	4.2	1.39 ± 0.32	14.0 ± 3.6
COSLA-17N	10 : 01 : 36.811	+ 02 : 11 : 09.66	4.6	4.2	3.55 ± 0.77	12.5 ± 3.2
COSLA-17S	10 : 01 : 36.772	+ 02 : 11 : 04.87	5.3	4.2	3.02 ± 0.57	12.5 ± 3.2
COSLA-18	10 : 00 : 43.190	+ 02 : 05 : 19.17	4.5	4.2	2.15 ± 0.48	10.0 ± 2.6
COSLA-19	10 : 00 : 08.226	+ 02 : 11 : 50.68	4.1	4.1	3.17 ± 0.76	6.7 ± 1.8
COSLA-23N	10 : 00 : 10.161	+ 02 : 13 : 34.95	7.3	3.9	3.42 ± 0.47	6.4 ± 1.6
COSLA-23S	10 : 00 : 10.070	+ 02 : 13 : 26.87	6.2	3.9	3.70 ± 0.60	6.4 ± 1.6
COSLA-35	10 : 00 : 23.651	+ 02 : 21 : 55.22	4.2	3.8	2.15 ± 0.51	8.2 ± 2.2
COSLA-38	10 : 00 : 12.590	+ 02 : 14 : 44.31	4.4	3.7	8.19 ± 1.85	5.8 ± 1.6
COSLA-47	10 : 00 : 33.350	+ 02 : 26 : 01.66	5.3	3.6	3.11 ± 0.59	9.0 ± 2.8
COSLA-54	09 : 58 : 37.989	+ 02 : 14 : 08.52	5.0	3.6	3.26 ± 0.65	11.6 ± 4.1
COSLA-128	10 : 01 : 37.990	+ 02 : 23 : 26.50	4.8	3.1	4.50 ± 0.94	11.0 ± 3.5

$S_{870} > 9$ mJy may represent a physical limit to the luminosity of a star-forming galaxy.

However, it is clear that this conclusion is at odds with the sample under study here, in which nine objects retain flux densities $S_{870} > 9$ mJy within a single component in the high-resolution interferometric follow-up. It also runs contrary to the results of various other SMA follow-up studies of SCUBA sources, which have generally suggested that (sub-)mm source multiplicity is rare (e.g. Downes et al. 1999; Iono et al. 2006; Younger et al. 2007, 2008, 2009; Cowie et al. 2009; Hatsukade et al. 2010).

A more detailed account of the ALESS results has now been published by Hodge et al. (2013), facilitating an assessment of the prevalence of multiplicity. In fact, contrary to the claims advanced in Karim et al. (2013, and repeated in the abstract of Hodge et al. 2013), the ALMA results show that significant multiplicity is not common at all, consistent with previous studies (including the sample under

Table 5. Spectroscopic redshifts ($z_{\rm spec}$), optical/near-infrared photometric redshifts ($z_{\rm phot}$), 'long-wavelength' (sub-)mm/radio redshift estimates ($z_{\rm LW}$), Smolcic et al. (2012) redshifts ($z_{\rm S}$) and our stellar masses calculations (M_*) for the (sub-)mm galaxies in our final 30-source COSMOS sample. Note that stellar masses can only be estimated for the 18 sources for which an optical/near-infrared counterpart was secured in the available imaging data. Errors on the photometric redshifts were derived from the redshift values corresponding to χ^2 values higher by $\Delta\chi^2 = 1$ from the minimum-χ^2 solution (see Appendix D) and these photometric redshift errors are propagated through to the derived random errors on the stellar masses (which they dominate). In the case of the Smolcic et al. (2012) redshifts, the values without errors are the optical spectroscopic redshifts for their chosen galaxy identifications (albeit we reject several of these as implausible for the (sub-)mm sources; see Fig. 4) and the two lower limits are mm-to-radio estimates (which are clearly consistent with our own estimates of $z_{\rm LW}$).

Source	$z_{\rm spec}$	$z_{\rm phot}$	$z_{\rm LW}$	$z_{\rm S}$	$\log_{10}(M_*/{\rm M}_\odot)$
AzTEC1	4.64	$4.46^{+0.29}_{-0.16}$	$4.20^{+0.33}_{-0.19}$	$4.26^{+0.17}_{-0.20}$	$11.30^{+0.04}_{-0.03}$
AzTEC2	–	–	$3.60^{+0.13}_{-0.18}$	1.125	–
AzTEC3	5.30	$5.45^{+0.10}_{-0.25}$	$4.40^{+0.35}_{-0.39}$	5.299	$10.93^{+0.01}_{-0.03}$
AzTEC4	–	$4.61^{+0.54}_{-0.61}$	$5.00^{+0.27}_{-0.43}$	$4.10^{+0.43}_{-1.11}$	$11.53^{+0.08}_{-0.10}$
AzTEC5	3.97	$4.19^{+0.26}_{-0.19}$	$2.90^{+0.10}_{-0.15}$	3.971	$11.49^{+0.04}_{-0.03}$
AzTEC6	–	–	$3.86^{+4.91}_{-0.92}$	0.802	–
AzTEC7	–	$1.76^{+0.09}_{-0.11}$	$2.00^{+0.10}_{-0.11}$	$2.30^{+0.10}_{-0.10}$	$11.56^{+0.03}_{-0.04}$
AzTEC8	3.18	$3.15^{+0.05}_{-0.15}$	$2.80^{+0.11}_{-0.10}$	3.179	$11.23^{+0.01}_{-0.03}$
AzTEC9	–	$4.85^{+0.50}_{-0.15}$	$4.60^{+0.50}_{-0.31}$	1.357	$11.02^{+0.07}_{-0.02}$
AzTEC10	–	$5.00^{+2.00}_{-0.50}$	$4.90^{+0.60}_{-0.41}$	$2.79^{+1.86}_{-1.29}$	$11.76^{+0.25}_{-0.08}$
AzTEC11	1.60	$1.64^{+0.06}_{-0.14}$	$2.40^{+0.11}_{-0.10}$	1.599	$10.95^{+0.02}_{-0.05}$
AzTEC12	–	$2.46^{+0.09}_{-0.06}$	$2.80^{+0.10}_{-0.10}$	$2.54^{+0.13}_{-0.33}$	$11.35^{+0.02}_{-0.02}$
AzTEC13	–	–	$4.70^{+1.25}_{-1.04}$	>3.59	–
AzTEC14	–	–	$3.38^{+1.00}_{-0.54}$	>3.03	–
AzTEC15	–	$2.43^{+0.32}_{-0.13}$	$3.90^{+0.59}_{-0.46}$	$3.01^{+0.12}_{-0.36}$	$11.19^{+0.08}_{-0.03}$
COSLA-5	–	–	$2.50^{+0.26}_{-0.17}$	$0.85^{+0.07}_{-0.06}$	–
COSLA-6N	–	–	$3.72^{+1.42}_{-0.63}$	$4.01^{+1.51}_{-0.83}$	–
COSLA-6S	–	–	$4.05^{+1.70}_{-0.71}$	$0.48^{+0.19}_{-0.22}$	–
COSLA-8	–	–	$1.90^{+0.11}_{-0.22}$	$1.83^{+0.41}_{-1.31}$	–
COSLA-16N	–	$2.21^{+0.14}_{-0.06}$	$2.30^{+0.10}_{-0.15}$	$2.16^{+0.12}_{-0.25}$	$11.38^{+0.04}_{-0.02}$
COSLA-17N	–	$3.11^{+0.09}_{-0.11}$	$4.70^{+0.51}_{-0.34}$	$3.37^{+0.14}_{-0.22}$	$11.09^{+0.02}_{-0.02}$
COSLA-17S	–	–	$3.94^{+1.64}_{-0.70}$	$0.70^{+0.21}_{-0.22}$	–
COSLA-18	–	$1.97^{+0.18}_{-0.27}$	$2.50^{+0.10}_{-0.14}$	$2.90^{+0.31}_{-0.43}$	$11.37^{+0.05}_{-0.08}$
COSLA-19	–	–	$3.50^{+0.34}_{-0.34}$	$3.98^{+1.62}_{-0.90}$	–
COSLA-23N	–	$4.29^{+0.31}_{-0.89}$	$3.70^{+0.22}_{-0.12}$	$4.00^{+0.67}_{-0.90}$	$11.53^{+0.05}_{-0.16}$
COSLA-23S	–	–	$4.80^{+2.25}_{-0.86}$	$2.58^{+1.52}_{-2.48}$	–
COSLA-35	–	$3.16^{+0.24}_{-0.26}$	$3.10^{+0.31}_{-0.16}$	$1.91^{+1.75}_{-0.64}$	$11.46^{+0.05}_{-0.06}$
COSLA-47	–	$3.32^{+0.13}_{-0.32}$	$2.40^{+0.12}_{-0.12}$	$2.36^{+0.24}_{-0.24}$	$11.54^{+0.03}_{-0.07}$
COSLA-54	–	$3.15^{+0.05}_{-0.15}$	$3.10^{+0.18}_{-0.11}$	$2.64^{+0.38}_{-0.26}$	$11.62^{+0.01}_{-0.03}$
COSLA-128	–	–	$4.90^{+2.27}_{-0.90}$	$0.10^{+0.19}_{-0.00}$	–

study here). Specifically, for the 20 brightest LESS sources for which Hodge et al. (2013) report ALMA results, only 5 reveal multiple ALMA subcomponents, and in only 2 of these 5 does the secondary component contribute >20 per cent of the flux density, thereby potentially significantly distorting the flux density and/or position of the original single-beam LABOCA source. Moreover, table 3 from Hodge et al. (2013) confirms that for the brightest 20 LESS sources, the radio identification technique in fact already yielded the correct galaxy counterpart in 17/20 cases (Biggs et al. 2011).

Thus, the ALMA results in fact confirm that multiplicity is *not* common, with only ≃10 per cent of bright sources showing a significant (e.g. >20 per cent) flux contribution from a secondary component. This result is confirmed by recent reports of SMA follow-up of SCUBA2 sources, which conclude that only ≃12 per cent of the 850 μm sources in SCUBA2 samples arise from blends of multiple fainter sources (Chen et al. 2013).

In the present study, we have also investigated whether there is any evidence that, on average, a significantly less (sub-)mm flux density is returned by the interferometric observations as compared to the original single-dish measurements. Here this is complicated by the fact that the AzTEC sources were followed up with (SMA) interferometry at shorter wavelengths, while the COSMOS LABOCA (COSLA) sources were followed up with (PdBI) interferometry at longer wavelengths. However, at least this brings some symmetry to the problem, potentially ameliorating somewhat any biases introduced by an incorrect choice of long-wavelength SED when performing the necessary *K*-corrections. In addition, we have performed this test with two different long-wavelength SED templates. Using the average SMG template described in Section 4.1 (applied at the relevant redshifts), we find that the mean interferometric/single-dish flux-density ratio for the 30 sources is $F_{\rm int}/F_{\rm single} = 0.96 \pm 0.09$ (median $F_{\rm int}/F_{\rm single} = 0.89$). Using an Arp 220 template, we find that mean $F_{\rm int}/F_{\rm single} = 0.98 \pm 0.08$ (median $F_{\rm int}/F_{\rm single} = 0.90$). Thus, while we acknowledge that the current sample is not ideal for this test, we find no significant evidence that either multiplicity or very extended emission is (on average) present at a level than can distort the true flux density of the sources in the large-beam single-dish measurements (at least with the beam sizes utilized here) by more than ≃10 per cent.

In summary, it now appears extremely unlikely that the number counts of (sub-)mm sources derived from single-dish surveys (e.g. Coppin et al. 2006; Austermann et al. 2010; Scott et al. 2012) have been significantly distorted by source blending, and the new interferometry results reinforce the success of previous galaxy counterpart identification programmes which have concluded that ≃80 per cent of (sub-)mm sources can have their galaxy counterparts correctly identified via sufficiently deep ancillary radio and/or *Spitzer* data. For completeness, we now explore this issue further, focusing on what conclusions would be drawn from the 30-source sample considered here, both with and without the extra information provided by interferometric follow-up.

5.2 The reliability of (sub-)mm galaxy identifications

Given the aforementioned success of the pre-ALMA LESS identification programme (Biggs et al. 2011), it is of interest to consider the extent to which the galaxy counterparts in the present COSMOS (sub-)mm sample would have been successfully identified without the assistance of the SMA and PdBI interferometric follow-up.

In the 15 years since the discovery of (sub-)mm sources, several methods have been proposed to identify their galaxy counterparts in the face of the relatively poor positional accuracy provided by single-dish (sub-)mm imaging. As already discussed, deep radio [generally 1.4 GHz Very Large Array (VLA)] imaging and deep mid-infrared [generally 24 μm *Spitzer* the multiband imaging photometer (MIPS)] imaging have proved particularly powerful in identifying galaxy counterparts, due to the fact that these wavelengths also trace star formation activity (e.g. Ivison et al. 2010), provide improved positional accuracy (especially at radio wavelengths) and yield source densities on the sky which are generally low enough to yield statistically significant associations (e.g. Ivison et al. 2002, 2007; Dunlop et al. 2010; Biggs et al. 2011; Wardlow et al. 2011; Michałowski et al. 2012a; Yun et al. 2012). It has also been found that (sub-)mm sources generally display very red optical–infrared

($i - K$) colours (e.g. Smail et al. 2004; Ashby et al. 2006; Michałowski et al. 2012a; Yun et al. 2012), apparently caused by a combination of dust obscuration and the presence of underlying massive evolved stellar populations (Michałowski et al. 2012b). Finally, it is now also well established that (sub-)mm galaxies are among the brightest galaxies at rest-frame near-infrared wavelengths, again due to their large stellar masses. At high redshifts this manifests itself as (sub-)mm galaxies appearing to be among the apparently brightest objects in *Spitzer* 8 μm IRAC imaging (Pope et al. 2006, 2008; Dye et al. 2008; Hainline et al. 2009; Wardlow et al. 2011; Michałowski et al. 2012b; Targett et al. 2013).

In order to test these methods, we selected VLA 1.4 GHz, *Spitzer* MIPS 24 μm, IRAC 8 μm and red ($i - K > 2$) counterparts to the (sub-)mm galaxies in the COSMOS sample in a similar way to that presented in Michałowski et al. (2012a). Following the method outlined in Dunlop et al. (1989) and Ivison et al. (2007), we assessed the reliability of each potential galaxy identification by calculating the corrected Poissonian probability, p, that each association could have been occurred by chance given our search parameters. Specifically, we applied this technique to the original pre-interferometric (sub-)mm source detections, using a search radius of $r_s = 2.5 \times 0.6 \times \mathrm{FWHM}/(\mathrm{S/N})$, where FWHM is the full width at half-maximum of the single-dish beam and S/N is the signal-to-noise ratio of the original (deboosted) AzTEC or LABOCA detection.

Armed with interferometrically refined coordinates from the subsequent SMA and PdBI observations, we can here test the success/reliability of such multifrequency association methods directly.

The results of this test of the identification process are summarized in Table B1 (available in the online version). Additional details can be found in the caption to this table (see also the notes on individual objects in the online version), but the key result is that 16 of the 30 sources would have been successfully identified on the basis of the single-dish (sub-)mm positions and the available multifrequency follow-up imaging. These 16 objects (marked with asterisks in Table B1 available in the online version) are 15 of the 18 sources for which stellar masses are given in Table 3 (and for which the multifrequency photometry is provided in Tables B2 and B3 available in the online version), plus AzTEC2, which is a purely radio identification confirmed by the interferometric positions. This means that 16/19 = 84 per cent of the galaxy identifications achievable with the aid of the improved interferometric positional accuracy would be correctly identified on the basis of the original single-dish data. The three additional galaxy identifications secured with the aid of the SMA and PbBI data comprise new galaxy counterparts for COSLA-54 and COSLA-17N, and a revised identification for AzTEC15 where a surprisingly large positional shift is reported between the original AzTEC position and the SMA peak.

Interestingly, three further identifications suggested by the single-dish positions are formally excluded by the interferometric data, but without the new positions yielding a new alternative identification. In two of these cases (COSLA-5 and COSLA-8), the proposed single-dish identification was statistically compelling but now appears unacceptable given the reduced error on the mm position delivered by PdBI. One possible explanation of such apparently conflicting conclusions is that both these objects could be lensed, and that the optical–infrared counterpart yielding the statistically significant association is the lensing object. In our analysis we have, in effect, guarded against this possibility by adopting the long-wavelength redshift estimate for these objects. Finally, the apparently significant identification of COSLA-128 listed in the last row of Table B1 is formally excluded by the PdBI follow-up, but this is primarily because the PdBI position is $\simeq$11 arcsec from the LABOCA position (for reasons that are hard to explain).

In summary, while the interferometric observations clearly add important extra information on the AzTEC and LABOCA sources, for this luminous sample we find that $\simeq$80–85 per cent of the galaxy identifications which are achievable given the depth of the supporting multifrequency data would have been successfully secured without the aid of the interferometric follow-up. In other words, the main cause of failed identification is not blending or inadequate positional accuracy in the single-dish (sub-)mm positions, but supporting multiwavelength data of inadequate depth to reveal the galaxy counterparts of the more high-redshift sources in the current sample. Of course, as the supporting data become deeper, then the improved positional accuracy provided by interferometry (or, for example, SCUBA2 450 μm imaging) will become increasingly valuable as the source densities in the supporting data rise.

For completeness, we show in the online version, Figs C1 and C2, how the locations of the sources on the flux-density–redshift plane vary depending on whether one adopts the identifications based on single-dish or interferometric positions, and also whether one adopts the single-dish (Fig. C1) or interferometric (Fig. C2) flux densities. The average (sub-)mm flux density inferred from the interferometry is only $\simeq$10 per cent lower than the single-dish average, and in all four panels the average redshift of the identified sources lies just below $z = 3.5$ while the average redshift of the sources which currently lack optical–infrared is (as anticipated) slightly higher (but still at $z < 4$). It is thus unsurprising that our main science results are little changed by whether we adopt the single-dish or interferometric positions and flux densities in our analysis.

6 CONCLUSIONS

We have presented a new analysis of the brightest sample of unlensed (sub-)mm sources with existing (pre-ALMA) interferometric (SMA or PdBI) follow-up observations. Because these sources lie within the COSMOS field, we have been able to exploit the latest Subaru, UltraVISTA and *Spitzer* optical–infrared photometry to better establish their redshifts (z), stellar masses (M_*) and specific star formation rates (sSFR). We have also explored the extent to which the supporting data in the field could have been used to reliably identify the galaxy counterparts *without* the improved positional accuracy provided by sub-mm/mm interferometry. We find that the bright (sub-)mm sources in the COSMOS field display a redshift distribution indistinguishable from that of the lensed SPT sources (Vieira et al 2013), peaking at $z_{\mathrm{median}} \simeq 3.5$. We also find that the typical stellar mass of the most luminous (sub-)mm sources is independent of redshift for $z \simeq 2{-}5$, with median $M_* \simeq 2 \times 10^{11}\,\mathrm{M}_\odot$ assuming a Chabrier (2003) IMF. Consequently, their typical sSFR also remain approximately constant out to the highest redshifts probed, at $\mathrm{sSFR} \simeq 2.5\,\mathrm{Gyr}^{-1}$. We note that, consistent with recent ALMA interferometric follow-up of the LESS sub-mm sources (Hodge et al. 2013), and SMA follow-up of SCUBA2 sources (Chen et al. 2013), source blending is *not* a serious issue in the study of luminous (sub-)mm sources uncovered by ground-based, single-dish (FWHM < 18 arcsec) surveys; only $\simeq$10−15 per cent of bright ($S_{850} \simeq 5{-}10$ mJy) (sub-)mm sources arise from significant blends, and so the conclusions of our study are largely unaffected by whether we adopt the original single-dish mm/sub-mm flux densities/positions or the interferometric flux densities/positions. Our results suggest that apparent disagreements

over the redshift distribution of (sub-)mm sources are simply a result of 'down-sizing' in dust-enshrouded star formation, consistent with existing knowledge of the star formation histories of massive galaxies. They also indicate that bright (sub-)mm-selected galaxies at high redshift are, on average, subject to the same SFR-limiting processes as less luminous objects, and lie on the 'main sequence' of star-forming galaxies.

ACKNOWLEDGEMENTS

MPK acknowledges the support of the UK Science and Technology Facilities Council. JSD acknowledges the support of the Royal Society via a Wolfson Research Merit award, and the support of the European Research Council via the award of an Advanced Grant, and the contribution of the EC FP7 SPACE project ASTRODEEP (Ref. No: 312725). MJM acknowledges the support of the UK Science and Technology Facilities Council and the FWO Pegasus Marie Curie Fellowship. RAAB acknowledges the support of the European Research Council. MC acknowledges the support of the UK Science and Technology Facilities Council via an Advanced Fellowship.

This work is based in part on data products from observations made with ESO Telescopes at the La Silla Paranal Observatories under ESO programme ID 179.A-2005 and on data products produced by TERAPIX and the Cambridge Astronomy survey Unit on behalf of the UltraVISTA consortium. This study was based in part on observations obtained with MegaPrime/MegaCam, a joint project of CFHT and CEA/DAPNIA, at the Canada–France–Hawaii Telescope (CFHT) which is operated by the National Research Council (NRC) of Canada, the Institut National des Science de l'Univers of the Centre National de la Recherche Scientifique (CNRS) of France and the University of Hawaii. This work is also based in part on data products produced at TERAPIX and the Canadian Astronomy Data Centre as part of the Canada–France–Hawaii Telescope Legacy Survey, a collaborative project of NRC and CNRS. This work is based in part on observations made with the NASA/ESA *Hubble Space Telescope*, which is operated by the Association of Universities for Research in Astronomy, Inc., under NASA contract NAS5-26555. This work is also based in part on observations made with the *Spitzer Space Telescope*, which is operated by the Jet Propulsion Laboratory, California Institute of Technology under NASA contract 1407. We thank the staff of the Subaru telescope for their assistance with the z'-band imaging utilized here. This research has made use of the NASA/IPAC Infrared Science Archive, which is operated by the Jet Propulsion Laboratory, California Institute of Technology, under contract with the National Aeronautics and Space Administration.

REFERENCES

Amblard A. et al., 2010, A&A, 518, L9
Aretxaga I. et al., 2007, MNRAS, 379, 1571
Ashby M. et al., 2006, ApJ, 644, 778
Austermann J. E. et al., 2010, MNRAS, 401, 160
Barger A. J., Cowie L. L., Sanders D. B., Fulton E., Taniguchi Y., Sato Y., Kawara K., Okuda H., 1998, Nature, 394, 248
Biggs A. D. et al., 2011, MNRAS, 413, 2314
Bolzonella M., Miralles J., Pelló R., 2000, A&A, 363, 476
Bowler R. A. A. et al., 2012, MNRAS, 426, 2772
Bruzual G., Charlot S., 2003, MNRAS, 344, 1000
Calzetti D., Armus L., Bohlin R. C., Kinney A. L., Koornneef J., Storchi-Bergmann T., 2000, ApJ, 533, 682
Capak P. et al., 2008, ApJ, 681, L53
Capak P. et al., 2011, Nature, 470, 233
Chabrier G., 2003, ApJ, 586, L133
Chapin E. L. et al., 2009, MNRAS, 398, 1793
Chapman S. C., Blain A. W., Ivison R. J., Smail I. R., 2003, Nature, 422, 695
Chapman S. C., Blain A. W., Smail I., Ivison R. J., 2005, ApJ, 622, 772
Chen C.-C., Cowie L. L., Barger A. J., Casey C. M., Lee N., Sander D. B., Wang W.-H., Williams J. P., 2013, ApJ, 776, 131
Cirasuolo M. et al., 2007, MNRAS, 380, 585
Cirasuolo M., McLure R. J., Dunlop J. S., Almaini O., Foucaud S., Simpson C., 2010, MNRAS, 401, 1166
Clements D. L. et al., 2008, MNRAS, 387, 247
Combes F. et al., 2012, A&A, 538, L4
Coppin K. et al., 2006, MNRAS, 372, 1621
Coppin K. E. K. et al., 2009, MNRAS, 395, 1905
Cowie L. L., Barger A. J., Wang W.-H., Williams J. P., 2009, ApJ, 697, L122
Cox P. et al., 2011, ApJ, 740, 63
Daddi E. et al., 2009a, ApJ, 694, 1517
Daddi E., Dannerbauer H., Krips M., Walter F., Dickinson M., Elbaz D., Morrison G. E., 2009b, ApJ, 695, L176
Downes D. et al., 1999, A&A, 347, 809
Dunlop J. S., 2011, in Wang W., Lu J., Luo Z., Yang Z., Hua H., Chen Z., eds, ASP Conf. Ser. Vol. 446, Galaxy Evolution: Infrared to Millimeter Wavelength Perspective. Astron. Soc. Pac., San Francisco, p. 209
Dunlop J. S., Peacock J. A., Savage A., Lilly S. J., Heasley J. N., Simon A. J. N., 1989, MNRAS, 238, 1171
Dunlop J. S., Hughes D. H., Rawlings S., Eales S. A., Ward M. J., 1994, Nature, 370, 347
Dunlop J. S. et al., 2004, MNRAS, 350, 768
Dunlop J. S. et al., 2010, MNRAS, 408, 2022
Dye S. et al., 2008, MNRAS, 386, 1107
Gonzalez V., Labbé I., Bouwens R., Illingworth G., Franx G., Kriek M., Brammer G., 2010, ApJ, 713, 115
Gwyn S. D. J., 2011, preprint (arXiv:1101.1084)
Hainline L. J., Blain A. W., Smail I., Frayer D. T., Chapman S. C., Ivison R. J., Alexander D. M., 2009, ApJ, 699, 1610
Hatsukade B. et al., 2010, ApJ, 711, 974
Hayward C. C., Narayanan D., Keres D., Jonsson P., Hopkins P. F., Cox T. J., Hernquist L., 2013, MNRAS, 428, 2529
Hezaveh Y. D. et al., 2013, ApJ, 767, 132
Hodge J. A. et al., 2013, ApJ, 768, 91
Hughes D. H. et al., 1998, Nature, 394, 241
Hwang H. S. et al., 2010, MNRAS, 409, 75
Iono D. et al., 2006, ApJ, 640, L1
Ivison R. J. et al., 1998, ApJ, 494, 211
Ivison R. J. et al., 2002, MNRAS, 337, 1
Ivison R. J. et al., 2007, MNRAS, 380, 199
Ivison R. J. et al., 2010, MNRAS, 402, 245
Karim A. et al., 2013, MNRAS, 432, 2
Kennicutt R. C., 1998, ARA&A, 36, 189
Knudsen K. K., Neri R., Kneib J.-P., van der Werf P. P., 2009, A&A, 496, 45
Lindner R. R. et al., 2011, ApJ, 737, 83
Madau P., 1995, ApJ, 441, 18
McCracken H. J. et al., 2012, A&A, 544, 156
Michałowski M. J., Hjorth J., Watson D., 2010, A&A, 514, 67
Michałowski M. J. et al., 2012a, MNRAS, 426, 1845
Michałowski M. J., Dunlop J. S., Cirasuolo M., Hjorth J., Hayward C. C., Watson D., 2012b, A&A, 541, A85
Oke J. B., 1974, ApJS, 27, 21
Pope A. et al., 2006, MNRAS, 370, 1185
Pope A. et al., 2008, ApJ, 675, 1171
Riechers D. A. et al., 2010, ApJ, 720, L131
Riechers D. A. et al., 2013, Nature, 496, 329
Roseboom I. et al., 2013, MNRAS, 436, 430
Sanders D. B. et al., 2007, ApJS, 172, 86
Schinnerer E. et al., 2008, ApJ, 689, L5

Scott K. et al., 2008, MNRAS, 385, 2225
Scott K. S. et al., 2012, MNRAS, 423, 575
Simpson J. et al., 2014, ApJ, 788, 125
Smail S., Chapman S. C., Blain A., Ivison R. J., 2004, ApJ, 616, 71
Smolcic V. et al., 2011, ApJ, 731, L27
Smolcic V. et al., 2012, A&A, 548, 4
Stark D., Schenker M., Ellis R., Robertson B., McLure R., Dunlop J., 2013, ApJ, 763, 129
Swinbank A. M. et al., 2014, MNRAS, 438, 1267
Taniguchi Y. et al., 2007, ApJS, 172, 9
Targett T. A. et al., 2013, MNRAS, 432, 2012
Vieira J. D. et al., 2013, Nature, 495, 344
Wall J. V., Pope A., Scott D., 2008, MNRAS, 383, 435
Walter F. et al., 2012, Nature, 486, 233
Wang W., Cowie L., Barger A., Williams J., 2011, ApJ, 726, L18
Wardlow J. L. et al., 2011, MNRAS, 415, 1479
Weiss A. et al., 2009, ApJ, 707, 1201
Weiss A. et al., 2013, ApJ, 767, 88
Younger J. D. et al., 2007, ApJ, 671, 1531
Younger J. D. et al., 2008, MNRAS, 387, 707
Younger J. D. et al., 2009, ApJ, 704, 803
Yun M. S. et al., 2012, MNRAS, 420, 957

SUPPORTING INFORMATION

Additional Supporting Information may be found in the online version of this article:

Figure B1. Illustrates the galaxy identifications secured utilizing the accurate positions provided for the (sub-)mm sources by the SMA and PdBI interferometric observations, overlaying the SMA and PdBI positions on CFHT optical, UltraVISTA near-infrared and IRAC 8 μm image stamps.
Table B1. Summarizes the results of our attempt to establish galaxy identifications based on multi-frequency associations with the original single-dish (AzTEC and LABOCA) positions.
Tables B2 and B3. Provide the optical-infrared photometry for the 18 secure galaxy identifications (based on the interferometric positions) which was used to estimate the photometric redshifts and stellar masses given in Table 5.
(http://mnras.oxfordjournals.org/lookup/suppl/doi:10.1093/mnras/stu1402/-/DC1).

Please note: Oxford University Press are not responsible for the content or functionality of any supporting materials supplied by the authors. Any queries (other than missing material) should be directed to the corresponding author for the paper.

This paper has been typeset from a TEX/LATEX file prepared by the author.